Theory of Anisotropic Growth Rates in the Ordering of an fcc Alloy

R.J. Braun,* J.W. Cahn, G.B. McFadden, H.E. Rushmeier†
and A.A. Wheeler‡
National Institute of Standards and Technology
Gaithersburg, MD 20899
USA

March 19, 1997

Abstract

A multiple-order-parameter theory of ordering on a binary face-centered-cubic (fcc) crystal lattice is used to model diffuse interphase boundaries and provide expressions for the anisotropy of the kinetic coefficient that characterizes the speed of the order-disorder boundary. The anisotropy is varied parametrically with the ratio of two gradient energy coefficients. In contrast to the results from single-order parameter theories, the orientation dependence of the kinetic coefficient differs significantly from that of the surface energy. Although the interfacial free energy anisotropy from this model is not strong enough to eliminate any orientations in the (three-dimensional) equilibrium shapes, the kinetic coefficient is sufficiently anisotropic to eliminate some orientations during growth. The long-time kinetic growth shapes show the development of edges and corners in a definite sequence.

*Permanent address: Department of Mathematical Sciences, University of Delaware, Newark, DE, 19716

†Permanent Address: IBM, T.J. Watson Research Center, Yorktown Heights, NY 10598

‡Permanent address: Faculty of Mathematical Studies, University of Southampton, Highfield, Southampton, SO9 5NH, UK.

1. Introduction

Dynamic and energetic calculations carried out with free energy functionals using variational arguments for the evolution equations result in interface energies and mobilities that are isotropic in cubic systems unless special modifications are employed. When there is a single nonconserved scalar order parameter, the usual form of the resulting equation is the Cahn-Allen equation [1] describing antiphase boundary motion between domains of an ordered phase. For a single conserved parameter, such as the composition, the result is the Cahn-Hilliard equation [2, 3] used to describe the spinodal decomposition of a binary alloy. Phase-field descriptions of the solidification of binary alloys have been developed recently [4, 5, 6]; they can be viewed as combining elements of the Cahn-Allen and Cahn-Hilliard models. In many cases gradient energy models can be viewed as mean field approximations to models that provide atomic-level descriptions [7, 8, 9].

Crystalline anisotropy is an important component of many of these phase changes. Some types of anisotropy are associated with the interfaces, while others, such as anisotropic elastic effects (ignored in this work), are associated with the volumes, even when they arise from coherency constraints at interfaces [2]. Anisotropic interfaces occur naturally in atomic models of crystalline systems [10, 11]. The symmetry of a crystal imposes symmetry constraints on the properties of both bulk and interfacial properties [12]. For example, it is well known that the second rank diffusion tensor is constrained to be isotropic for a cubic material. In contrast, surface energies are generally not tensor properties, and even cubic crystals are expected to have anisotropic interfacial properties, consistent with the underlying symmetries.

There have been a variety of approaches for modeling anisotropy in such models. A computationally successful one [13, 14] makes the gradient energy coefficient be a function of the direction of the gradient in a way that the surface energy calculated from that model conforms to a given anisotropic function, ideally the empirical orientation dependent surface free energy γ, if it is known. A consequence of this method is that the mobility is found to have the same anisotropy as γ, unless a second anisotropic kinetic function is introduced as a multiplicative factor to match the interfacial mobility, if known. Recently we introduced a model with multiple order parameters that were based on the underlying crystallography, in particular for ordering of fcc to the $L1_2$ structure [15]. Since the ordering reaction generally produces a phase with symmetry properties that form a subgroup of those of the disordered phase, the symmetry properties for the interphase boundary (IPB) between the disordered fcc and ordered (Cu_3Au) phases are those of the ordered phase, which in this case is $m3m$ cubic. We found that an anisotropy in γ for the interphase boundaries (IPB) consistent with cubic symmetry was introduced naturally, even though this was a cubic to cubic transition and the gradient energy was proportional to quadratic terms in the gradients of the order parameters.

In this paper we use this model to construct a continuum kinetic formulation and examine the anisotropy of IPB motion kinetics. We briefly outline the derivation of the continuum gradient energy model in Section 2 (a more complete description is given elsewhere [15]) and use it to obtain, for all orientations, the orientation dependence of the structure and mobility of planar IPBs in Section 3.

2. Formulation

We consider a model for order-disorder transitions on an fcc crystal lattice, and describe the fcc crystal geometrically by four inter-penetrating simple cubic sublattices labeled 1, 2, 3, and 4, respectively (see Fig. 1). Site 1 is chosen to correspond to corners of the face-centered cube; sites 2, 3 and 4 correspond to the midpoints of the faces contained in the planes $x = 0$, $y = 0$ and $z = 0$, respectively. The overall state of the crystal is then assumed to be completely described by the four parameters $0 \le \rho_i \le 1$, $i = 1, 2, 3, 4$, representing the atomic fraction of A on each sublattice. Vacancies are neglected. For the AB_3 stoichiometry we will study, the atom fraction densities ρ_i must sum to unity.

It is convenient to introduce four parameters W, X, Y, and Z in place of the parameters ρ_i, defined by

$$W = \frac{1}{4}(\rho_1 + \rho_2 + \rho_3 + \rho_4), \tag{1a}$$

$$X = \frac{1}{4}(\rho_1 + \rho_2 - \rho_3 - \rho_4), \tag{1b}$$

$$Y = \frac{1}{4}(\rho_1 - \rho_2 + \rho_3 - \rho_4), \tag{1c}$$

$$Z = \frac{1}{4}(\rho_1 - \rho_2 - \rho_3 + \rho_4). \tag{1d}$$

The parameter W represents the atomic fraction of the overall system. In this paper we confine ourselves to the case of $W = 1/4$, and then X, Y and Z can vary between plus and minus one quarter. The nonconserved order parameters X, Y, and Z have a directional character; they measure differences in composition in adjacent (100), (010), and (001) planes, respectively. These order parameters can be considered the real parts of the [100], [010], and [001] composition modulations, respectively [16, 17]. The square of each order parameter is proportional to the intensity of the [100], [010], and [001] diffraction spots, respectively. In this model a disordered state is represented by $\rho_1 = \rho_2 = \rho_3 = \rho_4 = W$, which implies that $X = Y = Z = 0$. The use of these parameters is convenient, because, in contrast with the composition, which is rapidly varying in an ordered state, they may be slowly varying in space and therefore readily continuized [18].

The continuum treatment is based on a generalized free energy functional for an isothermal system, which is assumed to have the form

$$\mathcal{F} = \int_V \left\{ f(W, X_1, X_2, X_3) + \kappa(\nabla W)^2 + b_{jlkm} \frac{\partial X_j}{\partial x_l} \frac{\partial X_k}{\partial x_m} \right\} dV, \tag{2}$$

where for notational convenience the suffix notation is given by $X_1 = X$, $X_2 = Y$, $X_3 = Z$, and $(x_1, x_2, x_3) = (x, y, z)$; here we sum over repeated indices. The term $f(W, X_1, X_2, X_3)$ is the bulk Helmholtz free energy density, assumed given by a low order polynomial, and the remaining terms are gradient energy contributions, whose coefficients κ and b_{jlkm} are constants. The symmetries associated with the fcc crystal structure restrict the possible forms of f, κ, and b_{jlkm} [19].

We limit our attention to variations in the nonconserved order parameters and assume W is uniform in space and time, and restrict our attention to a free energy density $f(X, Y, Z)$ that is given by a fourth-degree polynomial. Imposing the appropriate symmetries for an fcc crystal implies that the energy can be written in the form

$$f(X,Y,Z) = a_2(X^2+Y^2+Z^2) + a_3XYZ + a_{41}(X^4+Y^4+Z^4) + a_{42}(X^2Y^2+X^2Z^2+Y^2Z^2); \tag{3}$$

as detailed in our earlier paper ([15] see also [20]). Here we have assumed that the energy is adjusted so that $f(0,0,0) = 0$. Note that symmetry permits the cubic term XYZ, which plays a fundamental role in the subsequent analysis.

Truncating the bulk free energy density at fourth degree is reasonable if the fourth-order terms are assumed positive definite; it is then possible to describe the equilibrium states in detail.[1] We will examine the behavior of equilibrium solutions and phase boundaries by prescribing the coefficients a_2, a_3, a_{41} and a_{42} themselves.

[1]To obtain a phase diagram in which the ordered and disordered phase with the same composition coexist in an equilibrium solution with such an expansion (called a congruent transition), it seems to be necessary not to have the fourth degree terms positive definite and continue to higher-degree terms; see the discussion in [15].

By requiring the gradient energy contribution to the free energy to be invariant under the symmetry operations of the fcc crystal, the number of independent coefficients in b_{jklm} reduces to two, and the square-gradient contribution can be written in the simple form [15]

$$b_{jlkm}\frac{\partial X_j}{\partial x_l}\frac{\partial X_k}{\partial x_m} = \frac{A}{2}\left(X_x^2 + Y_y^2 + Z_z^2\right) + \frac{B}{2}\left(X_y^2 + X_z^2 + Y_x^2 + Y_z^2 + Z_x^2 + Z_y^2\right) \tag{4}$$

$$= \frac{A-B}{2}\left(X_x^2 + Y_y^2 + Z_z^2\right) + \frac{B}{2}\left(|\nabla X|^2 + |\nabla Y|^2 + |\nabla Z|^2\right). \tag{5}$$

Here A and B are independent constants which can be interpreted as originating from first- and second-nearest neighbor interactions. The first group of terms in (5) is from nearest neighbor interactions and is responsible for the anisotropy; the second group is from second-nearest neighbor interactions and is isotropic [15, 20]. For $B/A = 1$ the interface is isotropic; we will investigate the anisotropy that results when $B/A < 1$.

2.1. Governing Equations

A simple set of dynamical governing equations can be obtained by writing $\tau \partial X_j/\partial t = -\delta\mathcal{F}/\delta X_j$, where τ is a phenomenological parameter, which for simplicity we will take to be constant. The system then evolves along paths of steepest descent of the functional $\mathcal{F}$. Evaluating the functional derivatives gives

$$\tau X_t = AX_{xx} + BX_{yy} + BX_{zz} - f_X, \tag{6a}$$

$$\tau Y_t = BY_{xx} + AY_{yy} + BY_{zz} - f_Y, \tag{6b}$$

$$\tau Z_t = BZ_{xx} + BZ_{yy} + AZ_{zz} - f_Z. \tag{6c}$$

For our purposes here it is sufficient to consider one-dimensional traveling wave solutions to these equations which represent a planar interfacial region. The order parameters only vary in a direction parallel to the unit normal to the interface, denoted by $\hat{\mathbf{n}} = (n_x, n_y, n_z)$, and we write $X_j(\mathbf{x}, t) = \hat{X}_j(\hat{\mathbf{n}}\cdot\mathbf{x} - Vt)$, with V to be determined. The governing equations then reduce to the form

$$-\tau V\frac{d\hat{X}_j}{d\zeta} = \lambda_j^2\frac{d^2\hat{X}_j}{d\zeta^2} - \frac{\partial f}{\partial \hat{X}_j}, \tag{7}$$

for $j = 1, 2, 3$, where $\zeta = \hat{\mathbf{n}}\cdot\mathbf{x} - Vt$, and $\lambda_j^2 = B + (A-B)n_j^2$ for $i = 1, 2, 3$. We subsequently omit the hat and write $\hat{X}_j(\zeta) = X_j(\zeta)$ to simplify the notation.

2.2. Bulk States

The disordered (fcc) state described by $X = Y = Z = 0$ is always a solution to the governing equations. For the bulk disordered phase to be stable (or metastable) we require that $a_2 > 0$. There are also spatially uniform ordered solutions of the form $X = Y = Z(\neq 0)$, where their common value, X, satisfies

$$2a_2 + a_3X + 4(a_{41} + a_{42})X^2 = 0, \tag{8}$$

which allows for two possible real values of X. Here we consider the case $a_3 < 0$, and denote the larger of the two roots by $X = \chi > 0$, which describes a stable ordered structure, the so-called Cu_3Au phase, which is also denoted by the Strukturbericht designation $L1_2$. For these solutions, $\rho_1 = W + 3\chi$ and $\rho_2 = \rho_3 = \rho_4 = W - \chi$, so that sites 2, 3, and 4 are identical, and are distinguished from site 1. The requirement that $0 \leq \rho_j \leq 1$ restricts the allowed values of X_j; we assume the coefficients a_2, a_3, a_{41}, and a_{42} have been chosen accordingly. The symmetries that correspond to changing the signs of two of the order parameters imply that there are related solutions of the form $X = \chi, Y = Z = -\chi$, and so forth. Other bulk states are possible in this model [15]; however, we do not consider those states in this paper. Here we consider solutions to the governing equations that represent an interphase boundary (IPB) separating a disordered bulk phase $X_j \to 0$ for $\zeta \to -\infty$ from an ordered Cu_3Au bulk phase with $X_j \to \chi$ as $\zeta \to +\infty$.

3. Results

As discussed in more detail below, if the bulk free energies of the two phases are equal, the surface energy associated with a stationary planar interface separating the phases can be computed, and the surface energy anisotropy can be determined as a function of the interface orientation. If the bulk free energies are unequal, then traveling wave solutions representing the transformation from one phase to the other can be obtained; in the limit that the energy difference between the bulk states is small, the front velocity is proportional to the energy difference and can be computed asymptotically to provide an expression for the kinetic anisotropy associated with the motion of the interface.

3.1. IPB Interfacial Energy Anisotropy

The equations (7) with $V = 0$ are Hamiltonian and have a first integral

$$\frac{\lambda_x^2}{2}[X_\zeta]^2 + \frac{\lambda_y^2}{2}[Y_\zeta]^2 + \frac{\lambda_z^2}{2}[Z_\zeta]^2 - f(X,Y,Z) = f_0, \tag{9}$$

where f_0 is a constant of integration. Inserting the far-field boundary conditions into this expression gives that

$$f(0,0,0) = f(\chi,\chi,\chi) = f_0, \tag{10}$$

For given values of a_3, a_{41}, and a_{42}, this coexistence occurs for values $a_2 = a_2^c$ and $\chi = \chi^c$ that satisfy Eq. (8) and the condition

$$3a_2^c + a_3\chi^c + 3(a_{41} + a_{42})[\chi^c]^2 = 0. \tag{11}$$

We therefore find that

$$a_2^c = \frac{a_3^2}{36(a_{41} + a_{42})}. \tag{12}$$

and

$$\chi^c = -\frac{6a_2^c}{a_3}. \tag{13}$$

In previous work [15] we have solved the ordinary differential equations for the one-dimensional IPB's between disorder and Cu_3Au using COLNEW [21], a boundary value problem solver and using finite difference methods.[2]

A sample of the structure of the interphase boundaries found in [15] is shown in Fig. 2; the order parameters have a separation of scale in their transition width which causes interfacial layering to occur that is reminiscent of the $L1_0$ (CuAu) structure, as found originally by Kikuchi and Cahn [22] using the cluster variation method. The conversion to occupation densities ρ_i shown in Fig. 3 allows for direct comparison with [22] as discussed in [15]. We show solutions for the (110) surface orientation in Fig. 4 for comparison. Kikuchi and Cahn give results for (100) and (110) IPB's; the method presented here has the advantage that IPB's for general orientations are easily computed,

[2] By appropriately rescaling the energy and the order parameters [15], we may work in dimensionless units with $a_{41} = 1$, $a_2^c = 1 + a_{42}$, $a_3 = -6a_2^c$, $\chi^c = 1$, and $A = 1$. The numerical calculations are performed in this dimensionless form, with the choice $a_{42} = 1$. For clarity, the results will be expressed in terms of the original, unscaled parameters a_2, a_3, a_{41}, and a_{42}.

and the model is easily extended to include dynamics. The behavior of the IPB profiles can be categorized based on the symmetry of the crystal lattice; for a discussion see [15].

Finel [23] has computed IPB profiles for fcc materials and has raised the question of whether second nearest neighbors are required, as in their tetrahedron-octahedron approximation. The gradient energy terms in our model can be interpreted as arising from continuizing a discrete internal energy based on first and second neighbor interactions [15]. However second neighbors are not taken into account in the entropy contribution to the free energy, and so our results appear much closer to those of the tetrahedron approximation of Kikuchi and Cahn [22].

It is possible to compute the excess free energy, and thus the interfacial energy caused by the presence of the gradients from one bulk state to the other. A number of equivalent expressions are available to evaluate the interfacial energy of a given IPB; the interfacial energy of the interface, γ, may be written as

$$\gamma(\vec{n}) = \int_{-\infty}^{\infty} \left\{ \frac{\lambda_x^2}{2}[X_\zeta]^2 + \frac{\lambda_y^2}{2}[Y_\zeta]^2 + \frac{\lambda_z^2}{2}[Z_\zeta]^2 + f(X,Y,Z) \right\} d\zeta, \tag{14}$$

where we recall that $\lambda_j^2 = B + (A-B)n_j^2$ depends on the components of the normal vector. On using the first integral, Eq. (9), we also have the form

$$\gamma = \int_{-\infty}^{\infty} \left\{ \lambda_x^2[X_\zeta]^2 + \lambda_y^2[Y_\zeta]^2 + \lambda_z^2[Z_\zeta]^2 \right\} d\zeta \tag{15}$$

We use trapezoidal rule integration with many points in the domain to accurately determine γ.

Contours of $\gamma(\vec{n})$ on a shaded sphere are shown in Fig. 5 for $B/A = 0.005$. The minimum interfacial energy (dark) occurs in the [100] directions and the maxima are in the [111] directions (light). This is in agreement with the results of Kikuchi and Cahn [22]; they found that $\gamma_{110} > \gamma_{100}$. This is not necessarily the ordering of the interfacial energy with orientation given by other methods as will be discussed later. For $B/A = .005$ we find that $\gamma_{111}/\gamma_{100} \approx 1.08$.

Using the vector thermodynamics of Cahn and Hoffman [24, 25, 26], it is possible to compute the equilibrium shape of an ordered particle of fixed volume (defined by a surface $\chi =$ constant) in a disordered solid from the calculated surface energy $\gamma(\vec{n})$. Because we are using a diffuse interface theory to compute the "boundary" between the two phases, there may be some question as to the meaning of the shape. We assume the (caliper) diameter of the shape is large compared to the interface thickness. We interpret this shape to be the shape of the level surface $X = 0.5\chi^c$, and this is justified on the basis of asymptotic analyses of models of these types [14, 25, 26]. The equilibrium shapes that we compute show a definite flattening in the [100] directions, thus tending toward a rounded cuboidal shape with no angular edges; see Figures 6(a) and 6(b).

The calculation of the interfacial energy for this diffuse-interface model does not require any asymptotic procedure; however, computation of the kinetic anisotropy of the growing ordered particle is conveniently done asymptotically. We first report the result of asymptotic analysis to determine the appropriate kinetic coefficient, and subsequently examine its anisotropy and resultant growth shapes.

3.2. Motion of an interphase boundary

We now consider the motion of an interphase boundary. Since the overall composition W is assumed constant in our model of the congruent transformation, boundary motion occurs via a local ordering process at the interface without the need for long-range diffusion to occur. To determine the form of the kinetic anisotropy, it suffices to compute the steady velocity of a one-dimensional front that propagates because of an energy difference between the bulk phases. We assume that the interphase boundary is close to equilibrium, and so we require a_2 to lie near a_2^c, so that $|a_2 - a_2^c|/a_2^c \ll 1$. The interface velocity is then found to be proportional to $(a_2 - a_2^c)$ to leading order, and an expansion gives a solvability condition at first order that takes the form

$$\tau V \int_{-\infty}^{\infty} \left([X_\zeta]^2 + [Y_\zeta]^2 + [Z_\zeta]^2\right)\, d\zeta = \delta f, \tag{16}$$

where $X(\zeta)$, $Y(\zeta)$, and $Z(\zeta)$ are the equilibrium layer solutions corresponding to $a_2 = a_2^c$, and

$$\delta f = \frac{[a_3]^2}{12(a_{41} + a_{42})^2}(a_2 - a_2^c) \tag{17}$$

is the free energy difference per unit volume between the ordered and disordered phases. If we write $\delta f = L_V(T - T_c)/T_c$, where L_V is the latent heat of transformation per unit volume, T is the temperature, and T_c is the congruent temperature, then the above relation can be expressed in the form $V = \mu(\hat{\mathbf{n}})(T - T_c)$, where the kinetic coefficient $\mu(\hat{\mathbf{n}})$ is defined by

$$\frac{1}{\mu(\hat{\mathbf{n}})} = \frac{\tau T_c}{L_V} \int_{-\infty}^{\infty} \left([X_\zeta]^2 + [Y_\zeta]^2 + [Z_\zeta]^2\right)\, d\zeta. \tag{18}$$

With our choice of far-field boundary conditions, the sign convention is consistent with transformation from the higher energy phase into the lower energy phase.

Note that the kinetic coefficient is a functional of the equilibrium solution IPB profiles whose form differs considerably from that of the interfacial energy (cf. Eq. (15)); this functional is the source for anisotropic kinetics which are distinct from the anisotropy of interfacial energy. This is in contrast to scalar diffuse-interface models of solidification with constant τ, wherein the resulting kinetic coefficient inherits the anisotropy of the interfacial energy [14]. This functional for μ will be shown to have much stronger anisotropy than the interfacial energy.

3.3. IPB Kinetic Anisotropy and Growth Shapes

Using the computed IPB profiles at each orientation, together with Eq. (18), we can now generate values of μ as a function of orientation. The kinetic coefficient $\mu(\vec{n})$ for $B/A = 0.005$, see Fig. 7, shows much more anisotropy than does $\gamma(\vec{n})$ (c.f. Fig. 7 and Fig. 5, and note the differences in the scales in the bars on the left). The minimum (maximum) μ is in the [100] ([111]) direction as in Fig. 5, but the variation of μ with orientation is much larger, as can be seen in Table 1. We can also compute a Cahn-Hoffman ξ-vector [24] for kinetics which we designate ξ_μ; in this case, the smallest convex portion of the surface determined by ξ_μ gives the long-time growth shape ("the ξ_μ surface") for the crystal in the absence of interfacial energy. This interpretation follows from the work of Frank [27], who developed this outlook to solve for the evolving shape. For a discussion of this interpretation with the method of characteristics, see e.g. Taylor, Cahn, and Handwerker [28].

We may increase the anisotropy by decreasing B/A and compute a different growth shape at each value of B/A. We find that for $B/A > 0.025$, there are no missing orientations in the long-time growth shapes; they are rounded cuboids with no angular edges. One such ξ_μ surface is shown in Fig. 8(a); here the ξ_μ surface and the growth shape are identical. The shape is flattened in the [100] directions because of the relatively slow growth in those directions.

For $0.025 > B/A > 0.01$ self-intersections in ξ_μ form about [110]; these self-intersections lead to volumes that have appearance of "ears." The self-intersections indicate that some orientations will disappear in "shocks" in the long-time growth shapes beginning from bounded initial shapes. The long-time growth shape is the convex surface that remains when when the "ears" are removed. The ξ_μ surface for $B/A = 0.015$ is shown in Fig. 8(b) and is representative of this range of B/A. In this range, the edges that have appeared have their biggest jump in slope at [110] and the jump in slope decreases to zero (the edge smooths out) before [111] is reached.

As B/A is decreased further, the ends of the edges split; this situation is depicted for $B/A = 0.009$ in Fig. 8(c). If the ears are removed, then the growth shape appears to have sharp edges that split near the [111] orientations and the "split ends" smooth out. The zoomed image in Fig. 8(c) shows the splitting and tapering off of the ears. The forked edges appear to point at each other in 3-fold symmetry about the [111] direction. Upon further decrease in B/A, the ends connect up to leave a rounded triangular facet about [111]. By $B/A = 0.008$, this connection has already occurred and a zoom of the ξ_μ surface in the vicinity of [111] is shown in Fig. 8(d). Further decrease in B/A results in larger ears along the same edges as shown in Fig. 8(e). In principle, the rounded triangular facet about [111] should shrink and disappear with decreasing B/A; however, we are unable to compute results for small enough B/A to see such behavior.

The long-time growth shapes we have shown develop missing orientations in the absence of interfacial energy. When surface energy is present and convex, the sharp edges that are predicted in the growth shape become energetically costly, and surface energy acts to round off these edges (see, e.g., Taylor *et al.* [28] and Yokoyama and Sekerka [29]).

4. Discussion

In this paper we have computed the orientation dependence of the interface kinetic coefficient μ of a planar interface between the disordered and ordered $L1_2$ phases for a model of an fcc alloy, or for a lattice gas model for a simple cubic solid growing from an fcc lattice fluid of the same density [30]. The kinetic coefficient is determined from an asymptotic analysis that relates interface velocity to the energy difference between the bulk phases. The anisotropies of this model are inherited from the underlying lattice and hence it is specific to fcc lattices. The analysis of ordering in an hcp system using the same methodology is currently being investigated [31].

We have displayed results in terms of growth shapes computed by using the method of characteristics; these figures represent the long-time, outward-growing shapes that result from bounded initial surfaces. The figures display ears for orientations that disappear in shocks, because of their rapid growth relative to nearby orientations. However, unlike the ears in the ξ-plot derived from anisotropic surface energies $\gamma(\vec{n})$, the kinetic ears shown here have significance: planar interfaces in ear orientations are stable in growth. In addition, these faster-growing directions actually dominate for inward growth and are a factor in the growth of saddle-shaped surfaces [28].

In the theory described in this paper there is a single anisotropy parameter given by the ratio B/A of the two coefficients that appear in the gradient energy expression. The anisotropic gradient energy can have many causes, but in this paper it is linked to first and second neighbor interaction energies. The same parameter, B/A, was used in the earlier paper [15] to calculate the orientation dependence of γ (see Table 1). Some numerical results for the surface energy and kinetic coefficient in terms of spherical harmonic expansion coefficients are given in the Appendix.

The multiple-order-parameter model provides expressions for the surface energy and kinetic coefficient that differ significantly in their relative levels of anisotropy. For phase-field models based on a scalar order parameter, anisotropy is typically introduced by assuming that the gradient energy coefficient and the mobility coefficient τ depend on the orientation of the level sets of the order parameter. To obtain independent variation of the surface energy and kinetic coefficient in these models, both the gradient energy coefficient and the mobility must be allowed to vary independently; in particular, if τ is constant the resulting kinetic coefficient μ is directly proportional to the surface energy γ [14]. For the multiple-order-parameter-model, cubic symmetry implies the isotropy of τ, and results in a one-parameter model for the simultaneous determination of both γ and μ. In this case the model predicts significant differences in the anisotropy of surface tension and interface kinetics, and we find that the orientation dependence of μ is considerably stronger than that of γ. We conclude that the proportionality implied by the single order parameter theory with isotropic τ is not a general result.

The progression of increasingly anisotropic growth shapes as B/A tends to zero goes though the following sequence: sphere ($B/A = 1$); to smooth cuboid; to cuboid with short sharp edge segments starting at <110> and progressing towards <111> without reaching it; then the edges fork; and later join to form a cuboid with curved triangular faces about <111>. Ultimately these faces shrink to form a sharp corners at <111>. This sequence of shape changes is an example of a sequence of a set of bifurcations and is characteristic of a number of physical applications with three-fold symmetry [32]. Note that the first orientations that disappear because of fast growth are the {110} planes, and not the faster growing {111} planes.

For relatively weak amounts of anisotropy in cubic systems, the symmetry of the anisotropy would be expected to correspond to that present in the first "Kubic harmonic" (sic) coefficient a_4 (see [33] and Appendix) that occurs in an expansion in terms of spherical harmonics. For weak anisotropy the maxima and minima that result then must occur at <111> and <100>, respectively, or vice versa, depending on the sign of the coefficient of the first Kubic harmonic in the expansion. There is a dichotomy for weak interface anisotropies in cubic systems that is based on this sign. The [111] IPB yields the highest surface energy and the fastest attachment kinetics; both γ and μ have the same negative sign for the first Kubic harmonic. The quantitative degree of anisotropy of the two differs by an order of magnitude. The variation can be more than 40% for kinetic anisotropy, and the long-time kinetic growth shapes are about to develop angular edges for $B/A = 0.025$; see Fig. 8(a) and Fig. 8(b). On the other hand, the equilibrium shape for $B/A = 0.025$ differs little from a sphere, being only slightly flattened in the [100] directions.

Results found in the solid-melt interfaces of fcc and bcc crystals are consistent with what is expected from mild anisotropy, but the sign of the anisotropy is different ($a_4 > 0$) from what we found. Experimentally, Camel et al. [34] found {111} (octohedroidal) flattening in equilibrium shapes and nonequilibrium shapes for fcc melt-solid interfaces, which is consistent with a sign for the first Kubic harmonic term that is opposite to our result. In their theoretical study of the nucleation kinetics of the liquid-solid bcc interface, Harowell and Oxtoby [35] found that the kinetic anisotropy was negligible close to the bulk melting point, while farther away it became pronounced. They found that growth in the [100] direction is faster than for [111]. Density functional theory was applied to the planar growth of an fcc solid into its melt in a low-index direction by Mikheev and Chernov [36]. They made a number of assumptions which essentially reduced the model to that of a Ginzburg-Landau approach; they found that for an fcc crystal, the kinetic anisotropy was roughly $\mu_{100}/\mu_{111} \approx 1.1$ to 1.2. Molecular dynamics simulations have been used to determine kinetic anisotropy; for a recent review see Gilmer [37]. Argon is also found to have $\mu_{100} > \mu_{111}$ with rather strong temperature dependence; Gilmer also points out that the molecular dynamics simulations find the kinetic anisotropy of argon could be as large as an order of magnitude, while the surface energy anisotropy was on the order of 5%. Although {111} growth forms were seen in NH_4Cl at high undercooling, the equilibrium and low undercooling forms were consistent with the positive Kubic harmonic [38].

If we use our results in a lattice gas model of the interface between a primitive cubic solid and a fcc lattice liquid, then the sign of the anisotropy we found ($a_4 < 0$), differs from that of the other cubic systems. A simple rationalization that this difference may be real is found by comparing the interplanar spacings (which are inversely proportional to the planar packing densities) of the (100) and (111) for the three cubic lattices. Primitive cubic differs from the fcc and bcc lattices in that the interplanar spacing for (100) is greater than for (111). Simple bond-counting models for low index faces gives an inverse correlation surface energy and interplanar spacing [10]. Some simple growth kinetics models, such as two dimensional nucleation and a recent theoretical study of plane front propagation in a two dimensional lattice [39], give similar correlations with interplanar spacing. Such rationalizations are based on discrete lattices, but our continuum model seems to be successful in retaining the correct signs of a lattice-based anisotropy.

Experimental results concerning the anisotropy of order-disorder IPB's in the solid state are relatively scarce and complicated by other factors, such as misfit, which affects morphology, and by compositions that are away from the congruent point, resulting in growth rates that are controlled by diffusion and which can cause morphological instabilities. A recent study of an fcc/$L1_2$ (γ/γ') multicomponent alloy system [40] was designed to eliminate misfit. They found equilibrium shapes that were slightly cuboidally distorted spheres. Because they expected the surface energy to be isotropic, they attributed this anisotropy to small residual misfit; our results indicate that the amount of misfit they found is in the expected range for surface energy anisotropy and with the expected sign. Their kinetic experiments were complicated by morphological instabilities, but in their micrographs, some growing particles have a clear cuboidal hull, and others have the appearance of beginnings of <111> dendrites. With the other sign of the anisotropy, octahedral hulls and <100> dendrites are expected for growth shapes.

To bolster the agreement with these experiments [40], we suggest further experiments to be conducted on a $L1_2$ system with a congruent point and no misfit:

1. We expect that there is a range of temperatures below the equilibrium ordering temperature where homogeneous nucleation will not take place, but instead heterogeneous nucleation will occur on defects and the bounding surface of a single crystal. In such situations the growth rates and shapes from well-separated nuclei could be measured.

2. Some solid state transformations are sufficiently fast that directional transformation can be studied by moving a specimen through a temperature gradient. Order disorder transformations may be in this category, because no long range diffusion is required.

The free energy functional that we employ is qualitatively correct at the congruent point of the fcc/L1_2 transition, but not at other points, since we have artificially insisted on the prevention of compositional segregation. We are currently working on improved models that employ a higher-order expansion for the bulk free energy density that would provide a better description of the phase diagram and would allow the effects of compositional segregation to be included.

The calculation of kinetic coefficients for our model is based on the steady motion of a planar interface; the description of nucleation kinetics, where surface energy plays a dominant role, would require calculations of a different nature than the ones presented here.

Acknowledgements

The authors are grateful for helpful discussions with Drs. D.M. Anderson, W.J. Boettinger, W.C. Carter, S.R. Coriell, R.P. McCormack and R.F. Sekerka. G.B.M. and J.W.C. were partially supported by the Applied and Computational Mathematics Program of DARPA. A.A.W. and G.B.M. were partially supported by a NATO collaborative research grant.

Appendix

If we describe the surface orientation in terms of a spherical coordinate system with polar angle θ, $0 \leq \theta \leq \pi$, and azimuthal angle ϕ, $0 \leq \theta \leq 2\pi$, then the surface energy and kinetic coefficient can be expanded in terms of spherical harmonics as

$$\frac{\gamma(\vec{n})}{\gamma^{[111]}} = \sum_{\ell=0}^{\infty} \left\{ a_\ell Y_{\ell,0}(\theta,\phi) + \sum_{m=1}^{\ell} \left[a^c_{\ell,m} Y^c_{\ell,m}(\theta,\phi) \right] \right\}, \tag{19}$$

and

$$\frac{\mu(\vec{n})}{\mu^{[111]}} = \sum_{\ell=0}^{\infty} \left\{ b_\ell Y_{\ell,0}(\theta,\phi) + \sum_{m=1}^{\ell} \left[b^c_{\ell,m} Y^c_{\ell,m}(\theta,\phi) \right] \right\}, \tag{20}$$

where the spherical harmonics are defined as

$$Y_{\ell,0} = \sqrt{\frac{(2\ell+1)}{4\pi}} P_\ell(\cos\theta), \tag{21}$$

$$Y^c_{\ell,m} = \sqrt{\frac{(2\ell+1)}{2\pi}\frac{(\ell-m)!}{(\ell+m)!}} P^m_\ell(\cos\theta)\cos m\phi. \tag{22}$$

and

$$P_\ell(\xi) = \frac{1}{2^\ell\,\ell!}\frac{d^\ell}{d\xi^\ell}(\xi^2-1)^\ell, \qquad P^m_\ell(\xi) = (1-\xi^2)^{m/2}\frac{d^m P_\ell(\xi)}{d\xi^m}, \tag{23}$$

for $0 \leq m \leq \ell$, where $P_\ell(\xi)$ is the Legendre polynomial of degree ℓ.

The Kubic harmonics are linear combinations of the spherical harmonics that have cubic symmetry [33]. The first five Kubic harmonics are given by

$$p_0(\theta,\phi) = Y_{0,0}, \tag{24}$$

$$p_4(\theta,\phi) = Y_{4,0} + \frac{5}{\sqrt{35}} Y^c_{4,4}, \tag{25}$$

$$p_6(\theta,\phi) = Y_{6,0} - \sqrt{7} Y^c_{6,4}, \tag{26}$$

$$p_8(\theta,\phi) = Y_{8,0} + \frac{238}{51\sqrt{77}} Y^c_{8,4} + \frac{1105}{51\sqrt{715}} Y^c_{8,8}, \tag{27}$$

$$p_{10}(\theta,\phi) = Y_{10,0} - \frac{462}{\sqrt{105105}} Y^c_{10,4} - \frac{187}{\sqrt{12155}} Y^c_{10,8}, \tag{28}$$

where we have chosen to normalize the Kubic harmonics so that the coefficient of the $m = 0$ term is unity in each expression. (There are two linearly independent Kubic harmonics of degree 12, see, e.g., [41].)

Since $\gamma(\vec{n})$ and $\mu(\vec{n})$ have cubic symmetry, the above spherical harmonic expansions (19) and (20) reduce to expansions in terms of Kubic harmonics. In particular, because of our normalization the surface energy expansion through degree 10 is characterized by the coefficients a_0, a_4, a_6, a_8, and a_{10},

$$\frac{\gamma(\vec{n})}{\gamma^{[111]}} = a_0 p_0 + a_4 p_4 + a_6 p_6 + a_8 p_8 + a_{10} p_{10} + \sum_{\ell=12}^{\infty} \left\{ a_\ell Y_{\ell,0}(\theta,\phi) + \sum_{m=1}^{\ell} \left[a^c_{\ell,m} Y^c_{\ell,m}(\theta,\phi) \right] \right\}, \quad (29)$$

and similarly

$$\frac{\mu(\vec{n})}{\mu^{[111]}} = b_0 p_0 + b_4 p_4 + b_6 p_6 + b_8 p_8 + b_{10} p_{10} + \sum_{\ell=12}^{\infty} \left\{ b_\ell Y_{\ell,0}(\theta,\phi) + \sum_{m=1}^{\ell} \left[b^c_{\ell,m} Y^c_{\ell,m}(\theta,\phi) \right] \right\}. \quad (30)$$

We note that an isotropic surface tension would have a single non-zero expansion coefficient given by $a_0 = 2\sqrt{\pi} \approx 3.545$. In Tables 2 and 3 we give the expansion coefficients through degree 10. In order to give an indication of the rate of convergence of the series, we also give the coefficients a_{20} and a_{30}. The coefficients were obtained numerically by using computed values of γ and μ that were tabulated in one degree increments in θ and ϕ for each value of B/A.

References

[1] S. M. Allen and J. W. Cahn, *Acta metall.* **27**, 1085 (1979).

[2] J. W. Cahn, *Acta Metall.* **9**, 795 (1961).

[3] J. E. Hilliard, in *Phase Transformations* (edited by H. I. Aaronson). Metals Park, Ohio: American Society of Metals (1970).

[4] A. A. Wheeler, W. J. Boettinger, and G. B. McFadden, *Phys. Rev.* **A45**, 7424 (1992).

[5] A. A. Wheeler, W. J. Boettinger, and G. B. McFadden, *Phys. Rev.* E **47**, 1893 (1993).

[6] J. A. Warren and W. J. Boettinger, *Acta metall. mater.* **43**, 689 (1995).

[7] L. D. Landau, in *Collected Papers of L. D. Landau*, (edited by D. ter Haar). Pergamon, London (1965).

[8] R. Evans, *Adv. Phys.* **28**, 143 (1979).

[9] David W. Oxtoby, in *Liquids, Freezing and Glass Transition. Les Houches, Session LI* (edited by J. P. Hansen, D. Levesque, and J. Zinn-Justin). Elsevier Science Publisher, Amsterdam (1991).

[10] C. Herring, *Phys. Rev.* **82**, 87 (1951).

[11] F. C. Frank, in *Metal Surfaces*, American Society of Metals (1962).

[12] J. F. Nye, *Physical Properties of Crystals*, Clarendon Press, Oxford, 1985.

[13] R. Kobayashi, *Physica D* **63**, 410 (1993).

[14] G. B. McFadden, A.A. Wheeler, R.J. Braun, S. R. Coriell, and R. F. Sekerka, *Phys. Rev. E* **48**, 2016 (1993).

[15] R.J. Braun, J.W. Cahn, G.B. McFadden and A.A. Wheeler, *Phil. Trans. Roy. Soc. (Lond.)*, in press.

[16] A. Khachaturyan, *Theory of Structural Transformations in Solids*, Wiley, New York, 1983.

[17] D. de Fontaine, *MRS Bulletin*, 16 (August 1996).

[18] J. W. Cahn and A. Novick-Cohen, *J. Stat. Phys.* **76**, 877 (1994).

[19] E. M. Lifshitz, *Fiz. Zh.* **7,61**, 251 (1942).

[20] Z.-W. Lai, *Phys. Rev. B* **41**, 9239 (1990).

[21] G. Bader and U. Ascher, *SIAM J. Sci. Stat. Comput.* **8**, 483 (1987); U. Ascher, J. Christiansen and R.D. Russell, *ACM TOMS* **7**, 209 (1981).

[22] Ryoichi Kikuchi and John W. Cahn, *Acta Metall.* **27**, 1337 (1979).

[23] A. Finel, in *Ordering and disordering in alloys* (edited by A. Yavari). Elsevier Applied Science, New York (1992).

[24] J.W. Cahn and D.W. Hoffman, *Acta Metall. Mater.* **22**, 1205 (1974).

[25] A.A. Wheeler and G.B. McFadden, *Eur. J. Appl. Math.* **7**, 367 (1996).

[26] A.A. Wheeler and G.B. McFadden, "On the notion of a ξ-vector and a stress tensor for a general class of anisotropic diffuse interface models," NISTIR 5848, and submitted to the *Proc. Roy. Soc. (London)*, Series A.

[27] F.C. Frank, in *Growth and Perfection of Crystals*, (edited by R.H. Doremus, B.W. Roberts, and D. Turnbull). Wiley, New York (1958).

[28] J.E. Taylor, J.W. Cahn and C.A. Handwerker, *Acta metall. mater.* **40**, 1443 (1992); see also J.W. Cahn, J.E. Taylor and C.A. Handwerker, in *Sir Charles Frank, OBE, FRS, An eightieth birthday tribute* (edited by R.G. Chambers, J.E. Enderby, A. Keller, A.R. Lang, and J.W. Steeds). Hilger, New York (1991).

[29] Etsuro Yokoyama and Robert F. Sekerka, *J. Crystal Growth* **125**, 389 (1992).

[30] John W. Cahn and Ryoichi Kikuchi, *Phys. Rev. B* **31**, 4300 (1985).

[31] Susan Han and G.B. McFadden, unpublished research.

[32] J.W. Cahn and W.C. Carter, unpublished research.

[33] F.C. von der Lage and H. A. Bethe, *Phys. Rev.* **71**, 612 (1947).

[34] D. Camel, J.P. Simon, and N. Eusthatopoulos, *Scripta Metall.* **14**, 1101 (1980).

[35] P.R. Harowell and D.W. Oxtoby, *J. chem. Phys.* **86**, 2932 (1987).

[36] L.V. Mikheev and A.A. Chernov, *J. Crystal Growth* **112**, 591 (1991).

[37] G.H. Gilmer, Atomic-scale models of crystal growth, Ch. 8, in *Handbook of Crystal Growth* vol. 1, ed. D.T.J. Hurle. Elsevier, Amsterdam (1993).

[38] S.-K. Chan, H.-H. Reimer, and M. Kahlweit, *J Crystal Growth* **32**, 303 (1976).

[39] John W. Cahn, John Mallet-Paret, and Erik S. Van Vleck, Traveling wave solutions for systems of ODE's on a two-dimensional spatial lattice, preprint (1996).

[40] M.F. Henry, Y.S. Yoo, D.Y. Yoon, and J. Choi, *Metall. Trans.* **24A**, 1733 (1993).

[41] D.D. Betts, A.B. Bhatia, and Max Wyman, *Phys. Rev.* **104**, 37 (1956).

B/A	$\gamma_{100}/\gamma_{111}$	$\gamma_{110}/\gamma_{111}$	μ_{100}/μ_{111}	μ_{110}/μ_{111}
1.000	1.0	1.0	1.0	1.0
0.250	0.984	0.996	0.950	0.986
0.100	0.960	0.990	0.873	0.966
0.025	0.932	0.983	0.747	0.942
0.015	0.925	0.982	0.707	0.937
0.010	0.921	0.981	0.678	0.934
0.005	0.917	0.981	0.634	0.931
0	0.913	0.981	0.575	0.928

Table 1: Ratios of the surface energies and kinetic coefficients as functions of the ratio B/A for various interface orientations. The last row for $B/A = 0$ is a parabolic extrapolation of the latter three values.

	B/A					
	1.0	0.250	0.100	0.025	0.010	0.005
a_0	3.545	3.522	3.491	3.458	3.447	3.442
a_4	0	$-1.134(10^{-2})$	$-2.737(10^{-2})$	$-4.614(10^{-2})$	$-5.223(10^{-2})$	$-5.454(10^{-2})$
a_6	0	$7.339(10^{-5})$	$1.029(10^{-4})$	$-1.526(10^{-4})$	$-3.520(10^{-4})$	$-4.511(10^{-4})$
a_8	0	$-1.599(10^{-4})$	$-9.300(10^{-4})$	$-2.968(10^{-3})$	$-4.043(10^{-3})$	$-4.555(10^{-3})$
a_{10}	0	$2.789(10^{-6})$	$5.852(10^{-6})$	$7.349(10^{-5})$	$-1.672(10^{-4})$	$-2.266(10^{-4})$
a_{20}	0	$3.147(10^{-8})$	$6.287(10^{-7})$	$2.019(10^{-5})$	$-5.741(10^{-5})$	$-9.055(10^{-5})$
a_{30}	0	$-1.497(10^{-9})$	$-2.778(10^{-9})$	$-2.095(10^{-7})$	$-1.736(10^{-6})$	$-4.398(10^{-6})$

Table 2: Spherical harmonic expansion coefficient for $\gamma(\vec{n})/\gamma^{[111]}$ as functions of the anisotropy level B/A.

	B/A					
	1.0	0.250	0.100	0.025	0.010	0.005
b_0	3.545	3.475	3.375	3.253	3.211	3.193
b_4	0	$-3.454(10^{-2})$	$-8.641(10^{-2})$	$-1.599(10^{-1})$	$-1.903(10^{-1})$	$-2.044(10^{-1})$
b_6	0	$3.523(10^{-4})$	$5.586(10^{-4})$	$-1.325(10^{-3})$	$-3.351(10^{-3})$	$-4.668(10^{-3})$
b_8	0	$-7.866(10^{-4})$	$-5.151(10^{-3})$	$-1.984(10^{-2})$	$-3.030(10^{-2})$	$-3.653(10^{-2})$
b_{10}	0	$2.073(10^{-5})$	$6.187(10^{-5})$	$-7.515(10^{-4})$	$-2.112(10^{-3})$	$-3.218(10^{-3})$
b_{20}	0	$-8.720(10^{-8})$	$-9.893(10^{-6})$	$-3.559(10^{-4})$	$-1.255(10^{-3})$	$-2.306(10^{-3})$
b_{30}	0	$7.540(10^{-10})$	$1.454(10^{-8})$	$-5.379(10^{-6})$	$-6.270(10^{-5})$	$-1.947(10^{-4})$

Table 3: Spherical harmonic expansion coefficient for $\mu(\vec{n})/\mu^{[111]}$ as functions of the anisotropy level B/A.

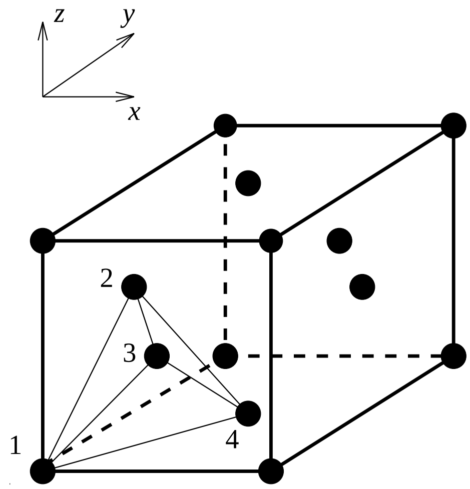

Figure 1: A schematic diagram of an fcc lattice. There are four distinguished sites corresponding to one at a corner and one each for the three faces intersecting at that corner.

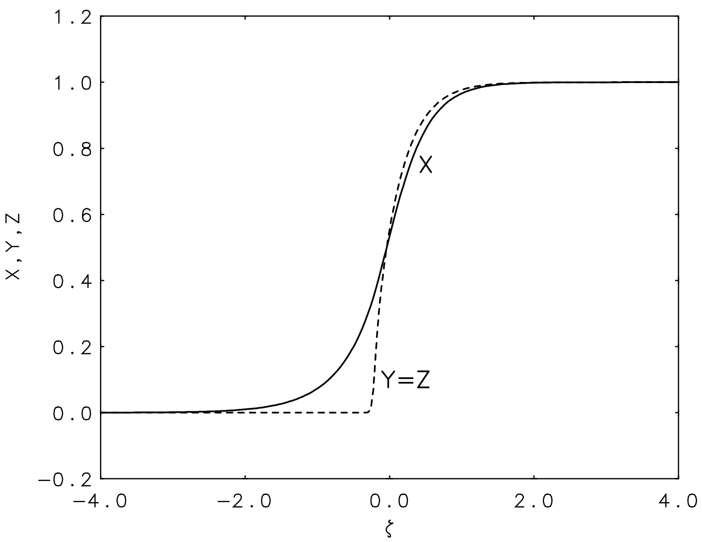

Figure 2: The order parameters, scaled to a maximum of unity, for the [100] orientation with $B/A = 0.005$. Note that $Y = Z$ for this orientation.

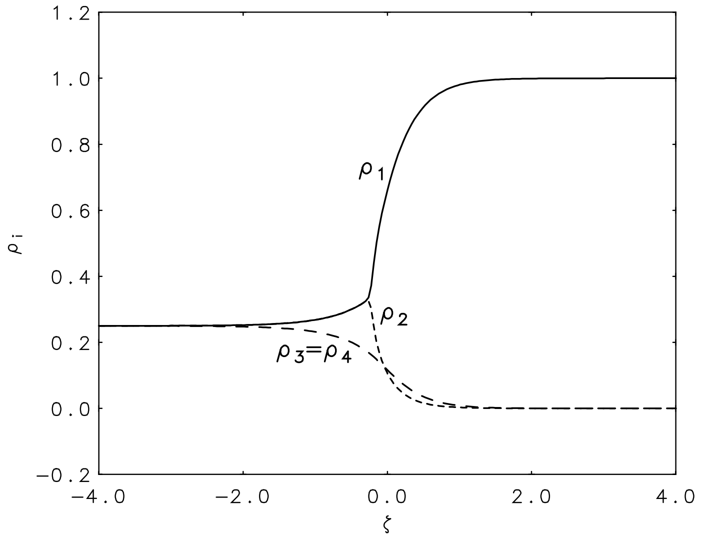

Figure 3: The sublattice atomic fractions ρ_i for $a_{42} = 1$, $B/A = 0.005$ for the [100] orientation.

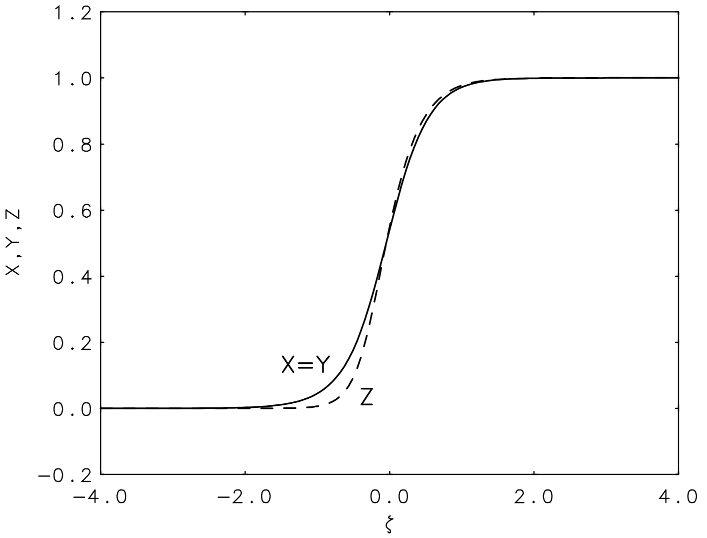

Figure 4: The order parameters, scaled to a maximum of unity, for the [110] orientation with $B/A = 0.005$. Note that $X = Y$ for this orientation.

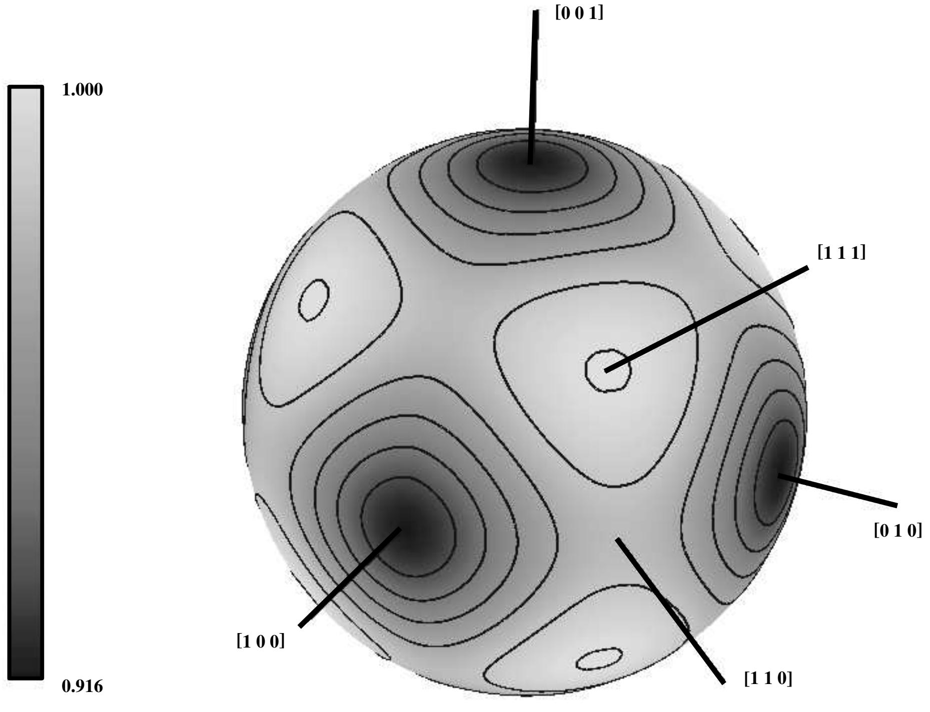

Figure 5: The relative variation of surface energy on the unit sphere for $B/A = 0.005$. The minima are in the <100> directions (dark) while the maxima (light, scaled to unity) are in the <111> directions (light).

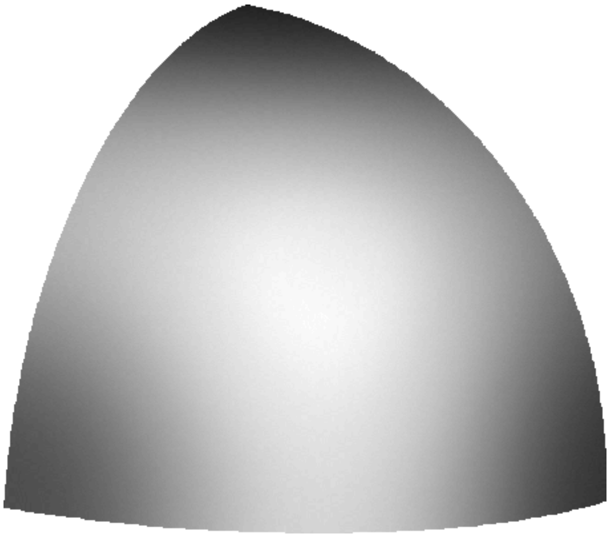

Figure 6(a): The isotropic ξ_γ surface $(B/A = 1)$ is simply a sphere and is shown for reference. The shading denotes the orientation with respect to the crystal lattice; here <100> is dark and <111> is light.

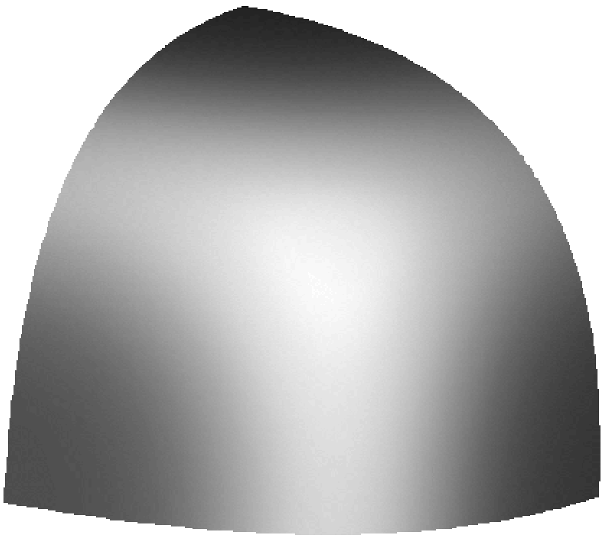

Figure 6(b): Equilibrium shape for $B/A = 0.005$. The equilibrium shape is not severely modified from a sphere, but there is definite flattening about the <100> orientations.

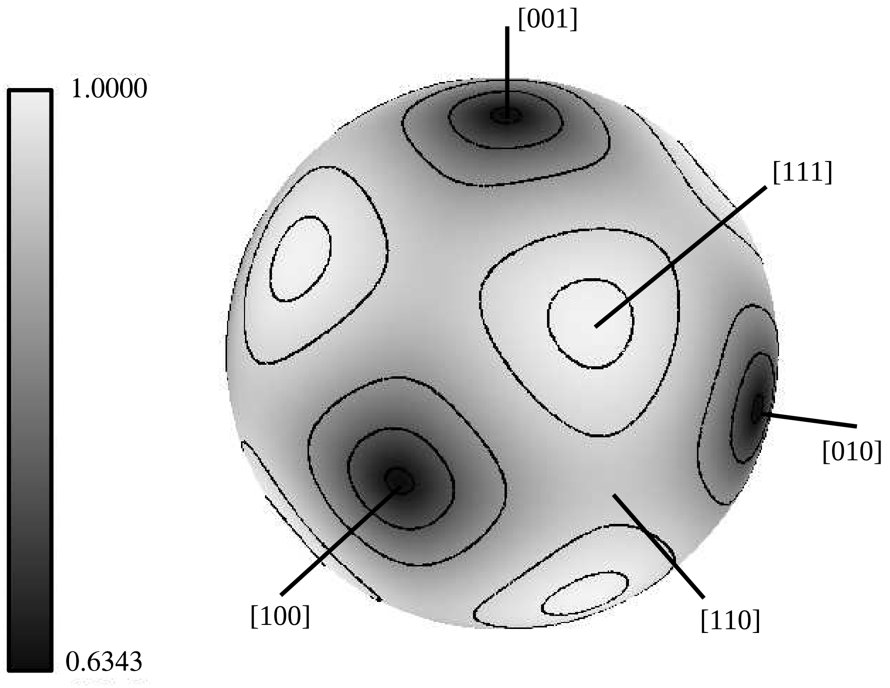

Figure 7: The relative variation of the kinetic coefficient on the unit sphere for $B/A = 0.005$ The minima are in the <100> directions (dark) while the maxima (light, scaled to unity) are in the <111> directions (light).

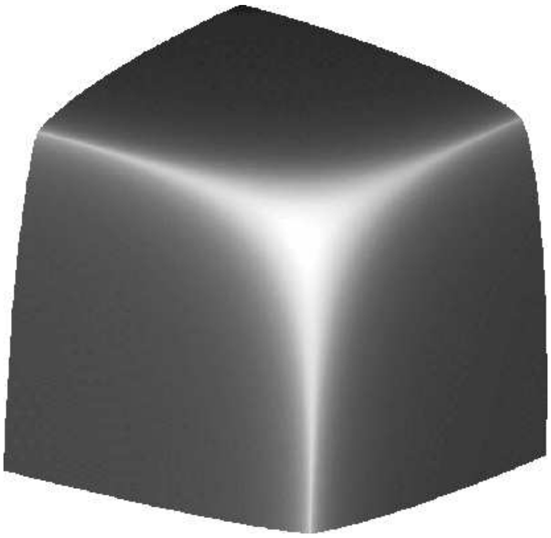

Figure 8(a): ξ_μ surface for $B/A = 0.025$. No edges have developed for this level of anisotropy, but the shape is strongly deformed from a sphere into a rounded cuboid. The slow-growing <100> and nearby orientations are clearly preferred.

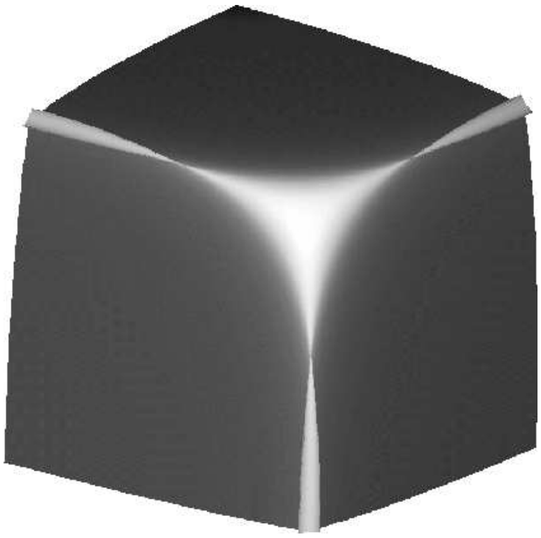

Figure 8(b): Here $B/A = 0.015$; edges have developed out of the [110] directions but they dissipate before reaching [111].

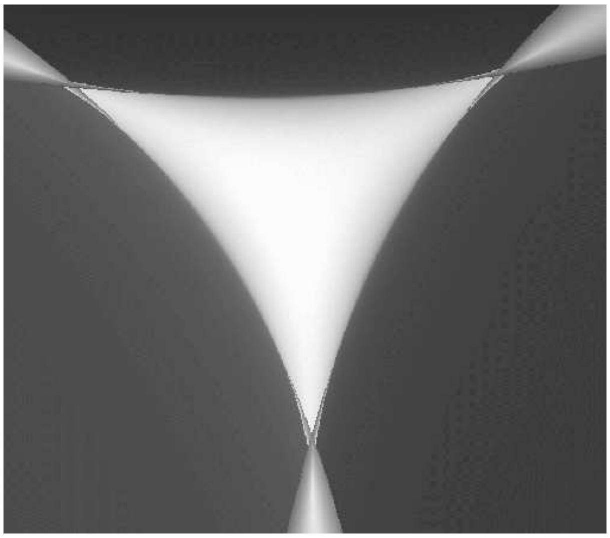

Figure 8(c): Zoom on the ξ_μ surface for $B/A = 0.009$ in the vicinity of [111]. In this view, it is clear that the now-forked edges have not joined up but dissipate before joining up around [111].

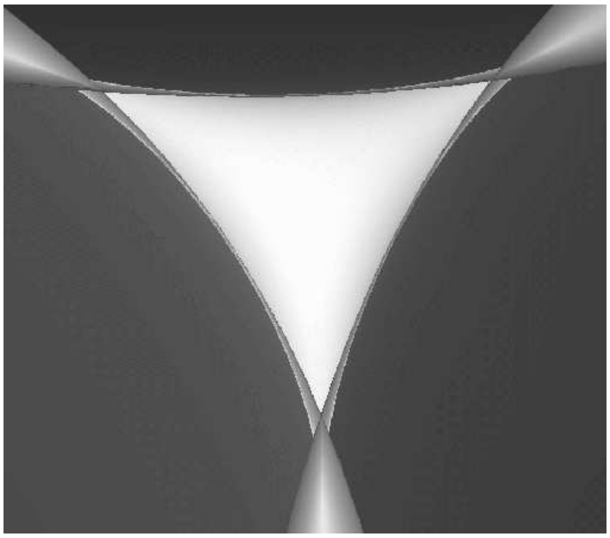

Figure 8(d): Zoom for $B/A = 0.008$ in the vicinity of [111]. The forked edges have now connected about [111]; the result is a rounded triangular facet in the growth shape when the ears are omitted.

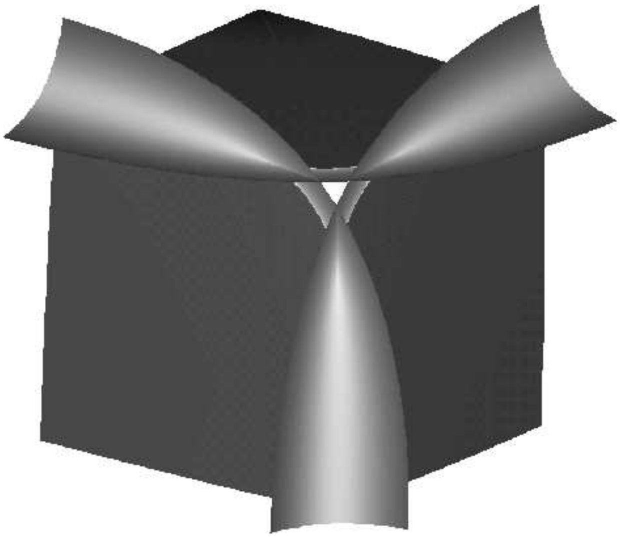

Figure 8(e): ξ_μ surface for $B/A = 0.005$. The growth in the size of the ears indicates the presence of sharper edges (larger jumps in slope).